INTERNATIONAL JOURNAL FOR NUMERICAL METHODS IN ENGINEERING
Int. J. Numer. Meth. Engng 2012; **92**:551–570
Published online 7 June 2012 in Wiley Online Library (wileyonlinelibrary.com). DOI: 10.1002/nme.4351

Relaxed incremental variational formulation for damage at large strains with application to fiber-reinforced materials and materials with truss-like microstructures

Daniel Balzani[1,*,†] and Michael Ortiz[2]

[1]*Institute of Mechanics, University of Duisburg-Essen, Faculty of Engineering, Department of Civil Engineering Universitätsstr. 15, 45117 Essen, Germany*
[2]*Engineering and Applied Sciences Division, California Institute of Technology, Pasadena, CA 91125, USA*

SUMMARY

In this paper, an incremental variational formulation for damage at finite strains is presented. The classical continuum damage mechanics serves as a basis where a stress-softening term depending on a scalar-valued damage function is prepended an effective hyperelastic strain energy function, which describes the virtually undamaged material. Because loss of convexity is obtained at some critical deformations, a relaxed incremental stress potential is constructed, which convexifies the original nonconvex problem. The resulting model can be interpreted as the homogenization of a microheterogeneous material bifurcated into a strongly and weakly damaged phase at the microscale. A one-dimensional relaxed formulation is derived, and a model for fiber-reinforced materials based thereon is given. Finally, numerical examples illustrate the performance of the model by showing mesh independency of the model in an extended truss, analyzing a numerically homogenized microtruss material and investigating a fiber-reinforced cantilever beam subject to bending and an overstretched arterial wall. Copyright © 2012 John Wiley & Sons, Ltd.

Received 27 October 2011; Revised 14 March 2012; Accepted 9 April 2012

KEY WORDS: incremental variational formulation; relaxation; damage; finite strains; fiber-reinforced materials; multiscale; homogenization

1. INTRODUCTION

The description of material deterioration plays an important role in a wide field of engineering applications. In particular, evolution processes at the microscale, such as growth, accumulation, and consolidation of voids, are assumed to be the main reasons for a macroscopically observable softening of the stress–strain response. For the phenomenological description of this phenomenon, very often approaches formulated in terms of continuum damage mechanics are used. Unfortunately, finite element calculations using such formulations typically lack from mesh-dependent solutions at certain deformation states. Another drawback might be that the damage evolution is taken into account at one scale only and that no direct link to an evolution of microstructure is possible. To overcome these difficulties, some approaches are given in the literature. As one of the first who interpreted damage as the homogenization of weakly and strongly damaged microphases, Francfort and Marigo [1] proposed a method based on the construction of a convex function (see also Francfort and Garroni [2] for an important extension combining quasistatic variational evolution with relaxation; for an application to fracture, see Francfort and Marigo [3]). The direct application of relaxation techniques to approaches formulated in terms of the classical continuum damage mechanics is given

*Correspondence to: Daniel Balzani, Institute of Mechanics, University of Duisburg-Essen, Faculty of Engineering, Department of Civil Engineering, Universitätsstr. 15, 45117 Essen, Germany.

†E-mail: daniel.balzani@uni-due.de

in Gürses [4]. There, the generalized variational approach from Miehe [5] is applied to damage, and mesh-independent solutions of finite element problems are shown when relaxed energies are used. An alternative approach using gradient enhancement is given in Dmitrievic and Hackl [6]. The latter publications are formulated for the small strain framework and do not directly apply for the physically and geometrically nonlinear case. Therefore, here, we focus on finite strains and derive an incremental variational framework in the sense of Ortiz and Repetto [7] and Ortiz and Stainier [8] for continuum damage mechanics using relaxed incremental energies. The relaxed model is obtained by numerically constructing a rank-one convex hull of the incremental formulation, which is considered to be a close approximation of the quasiconvex hull. Therefore, one advantage of the proposed formulation is that existence of minimizers of potential problems can be considered as given. This might also be important for the numerical solution of boundary value problems because mesh-independent solutions should be expected.

This paper is organized as follows. In Section 2, the mathematical framework is presented, where important details regarding continuum mechanics, continuum damage mechanics, and incremental variational formulations are recapitulated. Section 3 derives the proposed relaxed incremental variational formulation for damage making use of the classical (1-D) approach and provides an efficient framework for fiber-reinforced materials by applying a one-dimensional relaxation method to the fibers. In Section 4, numerical examples are given, where the proposed formulation is applied to the simulation of microtruss materials and fiber-reinforced materials. Section 5 concludes the paper.

2. MATHEMATICAL FRAMEWORK

In this section, the basic findings from continuum mechanics, incremental variational formulations, and continuum damage mechanics, which are required for the relaxed incremental variational formulation proposed in Section 3 and the examples provided in Section 4, are briefly recapitulated.

2.1. Continuum mechanics and invariant theory

Consider the physical body $\mathcal{B} \subset \mathbb{R}^3$, parameterized in $\boldsymbol{X}$, in the reference configuration and $\mathcal{B}_t \subset \mathbb{R}^3$, parameterized in $\boldsymbol{x}$, the body in the actual (deformed) configuration. The nonlinear deformation map $\boldsymbol{\varphi} : \mathcal{B} \to \mathcal{S}$ at time $t \in \mathbb{R}_+$ maps points $\boldsymbol{X} \in \mathcal{B}$ onto points $\boldsymbol{x} \in \mathcal{S}$. The deformation gradient $\boldsymbol{F}$ is then defined by

$$\boldsymbol{F}(\boldsymbol{X}) = \operatorname{Grad} \boldsymbol{\varphi}(\boldsymbol{X}), \qquad F^a{}_A = \frac{\partial x^a}{\partial X^A}, \tag{1}$$

with the Jacobian $J(\boldsymbol{X}) = \det \boldsymbol{F}(\boldsymbol{X}) > 0$. Another basic kinematic quantity, besides $\boldsymbol{F}$ and J, is the cofactor of $\boldsymbol{F}$, defined as $\operatorname{Cof} \boldsymbol{F} = \det \boldsymbol{F}\ \boldsymbol{F}^{-T}$. Note that the arguments $(\boldsymbol{F}, \operatorname{Cof} \boldsymbol{F}, \det \boldsymbol{F})$ represent the transformations of the infinitesimal line $\mathrm{d}\boldsymbol{X}$, area $\mathrm{d}\boldsymbol{A} = \boldsymbol{N}\, \mathrm{d}A$, and volume elements $\mathrm{d}V$ of the reference configuration to the infinitesimal line $\mathrm{d}\boldsymbol{x}$, area $\mathrm{d}\boldsymbol{a} = \boldsymbol{n}\, \mathrm{d}a$, and volume elements $\mathrm{d}v$ of the current configuration:

$$\mathrm{d}\boldsymbol{x} = \boldsymbol{F}\, \mathrm{d}\boldsymbol{X}, \quad \boldsymbol{n}\, \mathrm{d}a = \operatorname{Cof}[\boldsymbol{F}]\, \boldsymbol{N}\, \mathrm{d}A, \quad \text{and} \quad \mathrm{d}v = \det[\boldsymbol{F}]\, \mathrm{d}V, \tag{2}$$

where $\boldsymbol{N}$ and $\boldsymbol{n}$ are the normal vectors of the associated area elements. An important deformation measure for the construction of strain energy functions is the right Cauchy–Green tensor defined by

$$\boldsymbol{C} = \boldsymbol{F}^{\mathrm{T}} \boldsymbol{F}. \tag{3}$$

First, we concentrate on finite hyperelasticity, where the existence of a strain energy function $W := W(\boldsymbol{F})$ is postulated, and focus on strain energy functions $\psi := \psi(\boldsymbol{C})$ defined per unit reference volume in order to fulfill automatically the principle of material frame indifference. Then, the first Piola–Kirchhoff stresses, the second Piola–Kirchhoff stresses, and the Cauchy stresses can be computed from

$$\boldsymbol{P} = \frac{\partial W(\boldsymbol{F})}{\partial \boldsymbol{F}}, \quad \boldsymbol{S} = 2\frac{\partial \psi(\boldsymbol{C})}{\partial \boldsymbol{C}} = \boldsymbol{F}^{-1} \boldsymbol{P}, \quad \text{and} \quad \boldsymbol{\sigma} = \frac{1}{J} \boldsymbol{F}\, \boldsymbol{S}\, \boldsymbol{F}^{\mathrm{T}}, \tag{4}$$

DOI: 10.1002/nme

respectively. For a more convenient construction of reasonable strain energy functions, the invariant theory provides a suitable framework. For isotropy, the principle invariants are given by

$$I_1 = \operatorname{tr} \boldsymbol{C}, \quad I_2 = \operatorname{tr}[\operatorname{Cof} \boldsymbol{C}], \quad I_3 = \det \boldsymbol{C}, \tag{5}$$

and the energy function can be formulated as a function of these quantities $\psi := \psi(I_1, I_2, I_3)$.

2.2. Incremental variational formulations

With view to structural engineering problems, the aim is to compute the deformation field $\boldsymbol{\varphi}$ such that the potential

$$\Pi(\boldsymbol{\varphi}) := \int_{\mathcal{B}} W(\boldsymbol{F}(\boldsymbol{\varphi}))\,\mathrm{d}V + \Pi^{\mathrm{ext}}(\boldsymbol{t}(\boldsymbol{\varphi})) \tag{6}$$

becomes stationary under suitable boundary conditions. Herein, Π^{ext} is the external potential taking into account boundary tractions $\boldsymbol{t}$; thus, volume loads and acceleration terms are neglected. Formally, this can be recast as the global minimization problem

$$\inf_{\boldsymbol{\varphi}} \left[\Pi(\boldsymbol{\varphi}) \mid \boldsymbol{\varphi} = \hat{\boldsymbol{\varphi}} \text{ on } \partial\mathcal{B}_{\boldsymbol{\varphi}},\ \boldsymbol{t} = \hat{\boldsymbol{t}} \text{ on } \partial\mathcal{B}_{\sigma} \right], \tag{7}$$

wherein $\partial\mathcal{B}_{\varphi}$ and $\partial\mathcal{B}_{\sigma}$ describe the surfaces where tractions and deformations are prescribed, respectively. For inelastic solids, the strain energy density can be computed by the incremental variational problem

$$W(\boldsymbol{F}_{k+1}) = \inf_{\boldsymbol{q}}[\mathcal{W}(\boldsymbol{F}_{k+1}, \boldsymbol{q}_{k+1})] \quad \text{with} \quad \mathcal{W}(\boldsymbol{F}_{k+1}, \boldsymbol{q}_{k+1}) := \int_{t_k}^{t_{k+1}} (\dot{\psi} + \phi)\,\mathrm{d}t \tag{8}$$

describing the generalized work done in the material in the time increment $[t_k, t_{k+1}]$ under the initial boundary condition $\boldsymbol{q}(t_k) = \boldsymbol{q}_k$. Here, $\boldsymbol{q}$ denotes the generalized vector of internal variables describing the dissipative behavior. The energetic quantities ψ and ϕ denote the strain energy and the dissipation potential, respectively. Because of this pseudo-hyperelastic representation (in an incremental sense), the analysis of generalized convexity conditions known for the notion of hyperelasticity is enabled although the underlying strain energy function describes an inelastic material response. In particular, in the context of continuum damage mechanics usually, W is nonconvex as a result of the stress-softening behavior. This leads to a series of problems such as the existence of minimizers as well as material stability cannot be a priori guaranteed. However, in general, a quasiconvex or polyconvex hull may be constructed in order to overcome these difficulties. Because the quasiconvexity condition is rather difficult for the practical use and the rank-one convexity is known to be a close approximation (see, e.g., Silhavý [9]), rank-one convex hulls are often used and considered in this paper.

2.3. Continuum damage mechanics

The basic idea in the context of continuum damage mechanics is to consider deterioration of the material as a stress-softening behavior of the constitutive law. This can be achieved by taking into account an energy function of the type

$$\psi(\boldsymbol{C}, D) = (1 - D)\psi^0(\boldsymbol{C}), \tag{9}$$

wherein ψ^0 denotes the fictitiously undamaged effective hyperelastic strain energy density. Note that, because of objectivity, we focus on effective energy functions $\psi^0(\boldsymbol{C}) = \psi^0(\boldsymbol{F}^{\mathrm{T}}\boldsymbol{F}) =: \psi^0(\boldsymbol{F}, D)$, and whenever derivatives with respect to $\boldsymbol{F}$ are considered, appropriate transport relations are applied. Computing the time derivative of ψ and inserting in the Clausius–Duhem inequality for isothermal considerations leads to the equation for the stresses

$$\boldsymbol{S} = (1 - D)\boldsymbol{S}^0 \quad \text{with} \quad \boldsymbol{S}^0 = 2\partial_C \psi^0, \tag{10}$$

DOI: 10.1002/nme

and the reduced dissipation inequality reads

$$\phi := \psi^0 \, \dot{D} = \beta \dot{D} > 0 \,, \quad \text{with} \quad \beta = \psi^0 \tag{11}$$

being the thermodynamic force. The damage function $D \in [0, 1[$ is then assumed to be a monotonically increasing function of the thermodynamic force β. Here, we focus on damage evolving only during first loading cycles, which has been introduced as *discontinuous damage* in the sense of Miehe [10]. Therefore, we introduce the internal variable

$$\alpha_t := \max_{s \leqslant t} [\psi^0(\boldsymbol{C}_s)] \quad \text{for} \quad s, t \in \mathbb{R}^+, \tag{12}$$

describing the maximal value of effective energy reached up to the actual time, and reformulate the strain energy function

$$\psi(\boldsymbol{C}, \alpha) = (1 - D(\alpha))\psi^0(\boldsymbol{C}) \quad \text{with} \quad f := \psi^0 - \alpha \leqslant 0. \tag{13}$$

Herein, $f < 0$ describes the virtually hyperelastic regime. The damage function $D(\alpha)$ has to be constructed such that (11) is fulfilled. Note that, because of the existence of solely one internal variable, the generalized vector of internal variables $\boldsymbol{q}$ occurring in (8) consists only of α and is therefore a scalar.

3. RELAXED INCREMENTAL VARIATIONAL FORMULATION FOR DAMAGE

In this section, the framework for the description of damage at finite strains using incremental variational formulations is provided. In addition to that, a rank-one convex hull is constructed similar to the basic idea given in Francfort and Garroni [2], where the small strain framework has been considered. There, the idea was to consider macroscopic damage as a homogenization of micro-heterogeneously distributed damaged media. The increase of the volume fraction of the damaged media leads then to a macroscopic evolution of damage. Here, we consider a modification of this approach, which has also been taken into account in Gürses [4] for small strains. As long as the incremental variational problem remains rank-one convex, the original incremental variational model formulated in terms of the classical continuum damage mechanics is considered. Only if rank-one convexity is lost the relaxed energy is applied in order to furthermore guarantee the existence of minimizers.

3.1. General three-dimensional case

In case of damage evolution, the dissipation potential according to (11) is

$$\phi := \psi^0 \dot{D} = \alpha \, \frac{\partial D}{\partial \alpha} \, \dot{\alpha}. \tag{14}$$

For the time integration over the incremental step of the term $(8)_2$ partial integration is considered, that is,

$$\begin{aligned} \int_{t_k}^{t_{k+1}} \phi \, \mathrm{d}t &= \int_{\alpha_k}^{\alpha_{k+1}} \alpha \frac{\partial D}{\partial \alpha} \, \mathrm{d}\alpha = [\alpha \, D]\Big|_{\alpha_k}^{\alpha_{k+1}} - \int_{\alpha_k}^{\alpha_{k+1}} D(\alpha) \, \mathrm{d}\alpha \\ &= \alpha_{k+1} D(\alpha_{k+1}) - \alpha_k D(\alpha_k) - \bar{D}(\alpha_{k+1}) + \bar{D}(\alpha_k) \,, \end{aligned} \tag{15}$$

wherein $\bar{D}$ is the antiderivative of D. Then, the incremental stress potential in the actual time step is computed by

$$\begin{aligned} W(\boldsymbol{F}_{k+1}) &= \inf_{\alpha_{k+1}} \int_{t_k}^{t_{k+1}} [\dot{\psi}(\boldsymbol{F}_{k+1}, \alpha) + \phi(\boldsymbol{F}_{k+1}, \alpha)] \, \mathrm{d}t \\ &= \inf_{\alpha_{k+1}} [\Psi(\boldsymbol{F}_{k+1}, \alpha_{k+1})] \end{aligned} \tag{16}$$

DOI: 10.1002/nme

with the expression

$$\begin{aligned}\Psi(\boldsymbol{F}_{k+1},\alpha_{k+1}) = \psi(\boldsymbol{F}_{k+1},D(\alpha_{k+1})) - \psi(\boldsymbol{F}_k,D(\alpha_k))\\ + \alpha_{k+1}D(\alpha_{k+1}) - \alpha_k D(\alpha_k) - \bar{D}(\alpha_{k+1}) + \bar{D}(\alpha_k).\end{aligned} \tag{17}$$

In the sequel, we skip the index for the actual time step $(\cdot)_{k+1}$ if there is no danger of confusion. Then, the necessary condition

$$\begin{aligned}\partial_\alpha \Psi &= (\partial_D \psi(\boldsymbol{F},D))(\partial_\alpha D) + D(\alpha) + \alpha(\partial_\alpha D) - \partial_\alpha \bar{D}\\ &= \partial_\alpha D(\alpha - \psi^0) = 0\end{aligned} \tag{18}$$

leads to the actual internal variable

$$\alpha = \psi^0(\boldsymbol{F}), \tag{19}$$

for the case where damage evolution takes place. Finally, the incremental stress potential reads

$$W(\boldsymbol{F}) = \psi(\boldsymbol{F},D) - \psi(\boldsymbol{F}_k,D_k) + \alpha D - \alpha_k D_k - \bar{D} + \bar{D}_k\,, \tag{20}$$

with the abbreviations $D := D(\alpha)$, $D_k := D(\alpha_k)$, $\bar{D} := \bar{D}(\alpha)$, and $\bar{D}_k := \bar{D}(\alpha_k)$. The first Piola–Kirchhoff stresses are computed from the pseudo-hyperelastic formula

$$\partial_{\boldsymbol{F}} W + (\partial_D W)\,(\partial_\alpha D)\,(\partial_{\boldsymbol{F}}\alpha) = \partial_{\boldsymbol{F}} W + (\alpha - \psi^0)\,(\partial_\alpha D)\,(\partial_{\boldsymbol{F}}\alpha). \tag{21}$$

For the case when damage evolves, $\alpha = \psi^0$ holds; thus, the stresses are computed by

$$\boldsymbol{P} = \partial_{\boldsymbol{F}} W = (1-D)\partial_{\boldsymbol{F}}\psi^0. \tag{22}$$

The tangent moduli are obtained from

$$\partial^2_{\boldsymbol{F}\boldsymbol{F}} W + \left(\partial^2_{\boldsymbol{F}D} W\right)\,(\partial_\alpha D)\,(\partial_{\boldsymbol{F}}\alpha). \tag{23}$$

For the case of damage evolution, the explicit expression reads

$$\mathbb{A} = (1-D)\partial^2_{\boldsymbol{F}\boldsymbol{F}}\psi^0 - (\partial_\alpha D)\,(\partial_{\boldsymbol{F}}\psi^0)\otimes(\partial_{\boldsymbol{F}}\psi^0). \tag{24}$$

Note that the relations (22) and (24) only hold for the unrelaxed energy, that is, as long as W does not lose rank-one convexity. If that happens, the rank-one convex hull needs to be considered. An incremental stress potential W is said to be rank-one convex if

$$W(\xi\boldsymbol{F}^+ + (1-\xi)\boldsymbol{F}^-) \leqslant \inf_{\xi,\boldsymbol{F}^+,\boldsymbol{F}^-}[\bar{W}] \quad \text{with} \quad \bar{W}(\xi,\boldsymbol{F}^\pm) = \xi W(\boldsymbol{F}^+) + (1-\xi)W(\boldsymbol{F}^-) \tag{25}$$

holds for all deformations $\boldsymbol{F}^+$ and $\boldsymbol{F}^-$, which fulfill rank $[\boldsymbol{F}^+ - \boldsymbol{F}^-] \leqslant 1$ for $\xi \in [0,1]$. In order to make sure that $\boldsymbol{F}^+$ and $\boldsymbol{F}^-$ are rank-one connected, the general multiplicative ansatz

$$\boldsymbol{F}^\pm = \boldsymbol{F}\,\boldsymbol{L}^\pm \quad \text{with} \quad \left\{\begin{array}{l}\boldsymbol{L}^+ = \boldsymbol{1} + (1-\xi)\,\boldsymbol{d}\otimes\boldsymbol{n},\\ \boldsymbol{L}^- = \boldsymbol{1} - \quad \xi\,\boldsymbol{d}\otimes\boldsymbol{n}\end{array}\right. \tag{26}$$

can be considered. Herein, the two states $\boldsymbol{F}^+$ and $\boldsymbol{F}^-$ are parameterized in the phase fraction ξ, the polarization vector $\boldsymbol{d} := \boldsymbol{d}(d,\varphi_d,\vartheta_d)$, and the unit vector $\boldsymbol{n} := \boldsymbol{n}(\varphi_n,\vartheta_n)$, wherein d represents the magnitude of $\boldsymbol{d}$ (cf. Figure 1 for spherical coordinates). If condition (25) is violated, then the right-hand side serves as a rank-one convexification, and the convexified energy replacing the original nonconvex energy reads

$$W(\boldsymbol{F}) \Leftarrow W^{RC}(\boldsymbol{F}) = \inf_{\boldsymbol{r}}[\bar{W}] \quad \text{with} \quad \bar{W}(\boldsymbol{F},\boldsymbol{r}) = \xi W(\boldsymbol{F}^+(\boldsymbol{r})) + (1-\xi)W(\boldsymbol{F}^-(\boldsymbol{r})), \tag{27}$$

with the vector of the bifurcation parameters $\boldsymbol{r} = [\xi, d, \varphi_m, \vartheta_m, \varphi_n, \vartheta_n]^{\mathrm{T}}$.

Note that, for the unloading and reloading processes, where no damage evolution is assumed, the internal variable remains $\max_t[\psi^0]$ and D remains unchanged. Therefore, for unloading and reloading cycles, no incremental framework is required, and simply the softened strain energy function $W(\boldsymbol{F}) = (1-D)\psi^0(\boldsymbol{F})$ with constant D is considered. The associated first Piola–Kirchhoff stresses and moduli are calculated by

$$\boldsymbol{P} = (1-D)\partial_{\boldsymbol{F}}\psi^0 \quad \text{and} \quad \mathbb{A} = (1-D)\partial^2_{\boldsymbol{F}\boldsymbol{F}}\psi^0. \tag{28}$$

DOI: 10.1002/nme

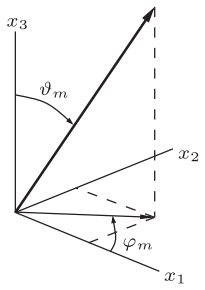

$$\boldsymbol{m}(\varphi_m, \vartheta_m) = \begin{pmatrix} \sin(\vartheta_m)\cos(\varphi_m) \\ \sin(\vartheta_m)\sin(\varphi_m) \\ \cos(\vartheta_m) \end{pmatrix}$$

Figure 1. Parameterization of the vector $\boldsymbol{m}$ in spherical coordinates.

3.2. Reduction to one-dimensional formulation

The minimization problem given in (25) and (27) is nonconvex, and usually, a large number of local minima exist. For that reason, the determination of the global minimum is rather difficult and, in most cases, expensive. Therefore, we focus here on an efficient approach able to describe microheterogeneous materials with fibrous or truss structures at the microscale and concentrate on the one-dimensional case. This formulation may then be used in models using numerical homogenization of microtruss microstructures in the sense of direct micro–macro transition procedures or phenomenological descriptions of fiber-reinforced materials.

3.2.1. Mathematical model. We consider the one-dimensional counterpart of the deformation gradient F and focus on the strain energy function

$$\psi(D, F) = (1 - D)\psi^0(F). \tag{29}$$

With the use of the results for the general three-dimensional case, the incremental stress potential

$$W(F) = \psi(F, D) - \psi(F_k, D_k) + \alpha D - \alpha_k D_k - \bar{D} + \bar{D}_k \tag{30}$$

is obtained. For the one-dimensional case, the rank-one convexity condition coincides with the convexity condition. Therefore, convexity of W with respect to F has to be checked. For that purpose, the actual deformation gradient is considered to be described by an interpolation between the two quantities F^+ and F^-, and then the ansatz (26) is adapted to the one-dimensional case, that is,

$$F := \xi F^+ + (1 - \xi)F^- \quad \text{with} \quad \begin{cases} F^+ := F(1 + (1 - \xi)d), \\ F^- := F(1 - \xi d). \end{cases} \tag{31}$$

Because the magnitude of the polarization vector $d = (F^+ - F^-)/F \in \mathbb{R}^+$ is mainly governed by the distance between F^+ and F^-, it can be interpreted as a measure for the intensity of microbifurcation into the strongly and weakly damaged phase. $\xi \in [0, 1]$ represents the volume fraction of the phase associated with F^+. Convexity of $W(F)$ requires that

$$W(\xi F^+ + (1 - \xi)F^-) \leqslant \inf_{\xi, d}[\xi W(F^+) + (1 - \xi)W(F^-)] \tag{32}$$

is satisfied. If this condition holds, then the stresses are computed from

$$P = (1 - D)\partial_F \psi^0 \tag{33}$$

and the tangent moduli can be calculated via

$$\mathbb{A} = (1 - D)\partial^2_{FF}\psi^0 - \partial_\alpha D\,(\partial_F \psi^0)^2. \tag{34}$$

If the condition does not hold, then the incremental stress potential needs to be convexified by setting

$$W \Leftarrow W_C(F) = \inf_{\xi, d}[\bar{W}(F, d, \xi)] \quad \text{with} \quad \bar{W} = \xi W(F^+) + (1 - \xi)W(F^-). \tag{35}$$

DOI: 10.1002/nme

Once ξ and d are identified from (35) at the situation where convexity becomes lost, F^+ and F^- are computed, and d can, from now on, be calculated by $d = (F^+ - F^-)/F$. This relaxed energy basically represents the volume average of the microscopic strain energy density governed by the bifurcation of the original homogeneous material into a highly and a weakly damaged phase. Then, ξ can be physically interpreted as the volume fraction of the phase whose physical behavior is described by the strain energy W^+. In case of tension, this means that W^+ is associated with the strongly damaged phase and W^- with the weakly damaged phase; for compression, vice versa.

3.2.2. Algorithmic treatment. The solution of the nonconvex minimization problem given in (32) or (35) is a challenging task and needs to be solved numerically. Here, we focus on the Newton scheme in order to compute the local minima according to a given start value in an efficient way because this method is known to converge quadratically in the vicinity of the solution. For obtaining the global minimum, a series of different starting values is chosen, and for each of them, a Newton iteration is performed. Then, the bifurcation parameters ξ and d leading to the lowest value of $\bar{W}$ are considered to be the minimizers. Of course, this does not guarantee the global minimum, but numerical analysis show that reasonable results are obtained. In addition to that, physically relevant bounds for the initial values of the bifurcation parameters can be defined to increase the potential of finding the global minimum.

The set of starting values is chosen by defining a grid of $N_\xi \times N_d$ bifurcation parameters ξ_i^{ini} and d_j^{ini} with the predefined minimum and maximum values $\xi_{\min}$, $\xi_{\max}$, $d_{\min}$, and $d_{\max}$, such that

$$\begin{aligned} \xi_i^{\text{ini}} &= \xi_{\min} + i(\xi_{\max} - \xi_{\min}), \quad \text{for} \quad i \in [0, N_\xi], \\ d_j^{\text{ini}} &= d_{\min} + j(d_{\max} - d_{\min}), \quad \text{for} \quad j \in [0, N_d]. \end{aligned} \tag{36}$$

In order to increase efficiency, suitable bounds should be defined. Where, for the volume fraction ξ, the minimum value is obviously $\xi_{\min} = 0$ and the maximum value $\xi_{\max} = 1$, the definition of reasonable bounds for d is not straightforward. Because F^+ and F^- have to be greater than zero, from (31), we obtain that $d < 1/\xi$ and thereby the maximum value of d should be different for each starting value of ξ, that is, $d < d_{\max,i} = 1/\xi_i$. However, in the case of tension, this is a rather loose bound because ξ is considered to be small at the point where convexity becomes lost. Therefore, additionally, $d < d_{\max}$ should be taken into account, where $d_{\max}$ is still a predefined value that can be estimated by defining reasonable bounds $F_{\min}^-$ and $F_{\max}^+$ surrounding the actual deformation gradient F and then setting $d_{\max} := \left(F_{\max}^+ - F_{\min}^-\right)/F$. Note that, also for ξ, stronger bounds can be considered. Because the initial value of the volume fraction should be typically close to 0 if $F \geqslant 1$ (tension) and close to 1 if $F < 1$ (compression), we set $\xi_{\min} = 0$ and $\xi_{\max} = 0 + \epsilon$ for tension and $\xi_{\min} = 1 - \epsilon$ and $\xi_{\max} = 1$ for compression, with $\epsilon \ll 1$.

Given a set of relevant initial values of the bifurcation parameters, the associated local minima have to be computed. Therefore, the necessary condition

$$\partial_{\boldsymbol{r}} \bar{W} = \mathbf{0}, \tag{37}$$

is taken into account. To solve this equation, a Newton iteration is performed. In one iteration step, the first and second derivatives of the energy $\bar{W}$ with respect to the bifurcation parameters $\boldsymbol{r}$ have to be computed, and the actual bifurcation parameters are updated by

$$\boldsymbol{r} \Leftarrow \boldsymbol{r} - [\partial_{\boldsymbol{r}\boldsymbol{r}}^2 \bar{W}]^{-1} \partial_{\boldsymbol{r}} \bar{W}. \tag{38}$$

Then, the Newton-iteration has to be repeated until $\partial_{\boldsymbol{r}} \bar{W} < tol$, wherein *tol* should be a small number close to computer accuracy. The individual derivatives required for this procedure are given in Appendix A. Having the relaxed energy computed, that is, the microbifurcation parameters are identified, the macroscopic stresses and tangent moduli can be computed for the case where the original problem loses convexity. For the stresses, the first derivative of the convexified energy

$$\partial_F W_C = \partial_F \bar{W} + (\partial_{\boldsymbol{r}} \bar{W}) \cdot (\partial_F \boldsymbol{r}) \tag{39}$$

is computed, and by inserting the necessary condition $\partial_{\boldsymbol{r}} \bar{W} = \mathbf{0}$, we obtain for the stresses

$$\bar{P} = \partial_F \bar{W} = \xi P^+ + (1 - \xi) P^- + \xi(1 - \xi)\, d\, (P^+ - P^-). \tag{40}$$

DOI: 10.1002/nme

Herein, the abbreviations $P^+ := P(F^+)$ and $P^- := P(F^-)$ are used, wherein, in turn, $P(\cdot)$ is evaluated on the basis of (33). The second derivative of the convexified energy reads

$$\partial^2_{FF} W_C = \partial^2_{FF} \bar{W} + \left(\partial^2_{F\boldsymbol{r}} \bar{W}\right) \cdot (\partial_F \boldsymbol{r}). \tag{41}$$

The last term can be computed by the derivative of the linearized expression, which is given in (38), that is, $\partial_F \boldsymbol{r} = -\left(\partial^2_{\boldsymbol{r}\boldsymbol{r}} \bar{W}\right)^{-1} \left(\partial^2_{\boldsymbol{r}F} \bar{W}\right)$, and then the tangent moduli read

$$\bar{\mathbb{A}} = \partial^2_{FF} \bar{W} - \left(\partial^2_{F\boldsymbol{r}} \bar{W}\right) \cdot \left[\left(\partial^2_{\boldsymbol{r}\boldsymbol{r}} \bar{W}\right)^{-1} \left(\partial^2_{\boldsymbol{r}F} \bar{W}\right)\right]. \tag{42}$$

Note that this result is analogous to the one obtained for small strains (see Gürses [4]). The individual derivatives are provided in Appendix A, and a detailed description of the complete algorithm is given in Figure 2 and 3.

3.3. Formulation for unidirectionally reinforced materials

In many reinforced materials, the main load-bearing elements are the reinforcements; therefore, the main damage can be assumed there. On the basis of this assumption, an efficient three-dimensional relaxed variational damage formulation can be obtained by applying the one-dimensional model derived in the previous section to a unidirectional reinforcement, which is subsequently referred to as fiber reinforcement. Then, the overall strain energy function may be additively decoupled into an undamaged isotropic part for the matrix and the superposition of n_f transversely isotropic parts for

1) Get history variables α_k, ψ^0_k, α^+_k, $(\psi^0_k)^-$, α^+_k, $(\psi^0_k)^-$, ξ_k, d_k, F^+_k, F^-_k, $flag$
2) If $flag = 3$, set $flag = 1$
3) If $flag = 0$, then solve non-convex minimization problem:
   (Initialize $W_{min} = 1/tol$)
   - Loop over $i = 0..N_\xi$ and $j = 0..N_d$:
     - 3.1) Compute reasonable actual starting values ξ^{ini}_i, d^{ini}_j
     - 3.2) Newton iteration to find local minimum
       - Loop over l until $res < tol$ or $l = l_{max}$
         - 3.2.1) Compute $F^+ = F(1 + (1-\xi)d)$, W^+, P^+, $\mathbb{A}^+$
           $F^- = F(1 - \xi d)$, W^-, P^-, $\mathbb{A}^-$
         - 3.2.2) Compute homogenized energy $\bar{W} = \xi W^+ + (1-\xi)W^-$
         - 3.2.3) Get lower energy:
           if $\bar{W} < W_{min}$ then $W_{min} = \bar{W}$
           and save associated $\bar{\xi}$, $\bar{d}$
         - 3.2.4) Compute residual $res = |\partial_{\boldsymbol{r}} \bar{W}|$ and check:
           if $res < tol$ then goto 2.3
         - 3.2.5) Update bifurcation parameters $\boldsymbol{r} \Leftarrow \boldsymbol{r} - [\partial^2_{\boldsymbol{r}\boldsymbol{r}} \bar{W}]$
4) Compute ψ^0, α, $W(F)$, $P(F)$, $\mathbb{A}(F)$
5) If $flag = 1$, then compute actual volume fraction ξ based on the case distinction scheme, which is described in the algorithmic box shown in Fig. 3
6) If $flag = 1$, then compute $(\psi^0)^\pm$, $\alpha^\pm$, $W^\pm$, $P^\pm$, $\mathbb{A}^\pm$ and relaxed stresses and moduli via (40) and (42)
7) If $flag = 0$, then check for convexity: if $W_{min} < W$ then $flag = 3$
8) Set history variables: α_k, ψ^0_k, α^+_k, $(\psi^0_k)^-$, α^+_k, $(\psi^0_k)^-$, ξ_k, d_k, F^+_k, F^-_k, $flag$
   If $flag = 0$ or $flag = 2$ then $\alpha^\pm = \alpha$, $(\psi^0)^\pm = \psi^0$

Figure 2. Algorithmic box for the computation of the relaxed stresses and moduli; initial history values are zero.

DOI: 10.1002/nme

If $F \geqslant 1$ (tension) then:

If $\xi_k < tol$:

$$\xi = \begin{cases} 0 & \text{if} \quad F \leqslant F^- \\ (F - F^-)/(F^+ - F^-) & \text{if} \quad F^- < F < F^+ \end{cases}$$

Else If $tol \leqslant \xi_k < 1$:

$$\xi = \begin{cases} \xi_k & \text{if} \quad F \leqslant \xi_k F^+ (1 - \xi_k) F^- \\ (F - F^-)/(F^+ - F^-) & \text{if} \quad \xi_k F^+ (1 - \xi_k) F^- < F < F^+ \\ 1 \text{ and } flag = 2 & \text{if} \quad F \geqslant F^+ \end{cases}$$

Else $\xi = 1$

If $F < 1$ (compression) then:

If $\xi_k < tol$:

$$\xi = \begin{cases} 1 & \text{if} \quad F \geqslant F^+ \\ (F - F^-)/(F^+ - F^-) & \text{if} \quad F^- < F < F^+ \end{cases}$$

Else If $tol \leqslant \xi_k < 1$:

$$\xi = \begin{cases} \xi_k & \text{if} \quad F \geqslant \xi_k F^+ (1 - \xi_k) F^- \\ (F - F^-)/(F^+ - F^-) & \text{if} \quad F^- < F < \xi_k F^+ (1 - \xi_k) F^- \\ 0 \text{ and } flag = 2 & \text{if} \quad F \leqslant F^- \end{cases}$$

Else $\xi = 0$

Figure 3. Algorithmic box for the case distinction required for the calculation of the actual bifurcation parameter ξ.

the fibers (cf. Balzani *et al.* [11], where this structure has been used for the simulation of damage in arterial walls). The energy function is assumed to have the structure

$$\psi := \psi^{\text{iso}}(\boldsymbol{F}) + \sum_{a=1}^{n_f} \psi_{(a)}^{ti}(F_{(a)}, D_{(a)}) \quad \text{with} \quad \psi_{(a)}^{ti} = (1 - D_{(a)}(F_{(a)}))\psi_{(a)}^{0}(F_{(a)}), \tag{43}$$

wherein the transversely isotropic part is represented by the one-dimensional relaxed variational model. Therefore, the general three-dimensional deformation has to be mapped to the direction of the individual fiber reinforcement by setting $F_{(a)} = |\boldsymbol{a}_{(a)}|$, wherein the direction of the fiber reinforcement (a) in the actual (deformed) configuration is denoted by $\boldsymbol{a}_{(a)} = \boldsymbol{F}\,\boldsymbol{A}_{(a)}$ and in the reference configuration by $\boldsymbol{A}_{(a)}$. Then, the relaxed first Piola–Kirchhoff stresses $P_{(a)}$ and associated moduli $\mathbb{A}_{(a)}$ are calculated for the individual fiber reinforcements at the microscale. After pushing forward into the actual configuration by the relations

$$\tau_{(a)} = P_{(a)} F_{(a)} \quad \text{and} \quad \mathbb{c}_{(a)} = F_{(a)} \left(F_{(a)} \mathbb{A}_{(a)} - P_{(a)} \right) \tag{44}$$

the coefficients of the tensorial representations of the Kirchhoff stresses and associated moduli are

$$\tilde{\tau}_{(a)}^{11} = \tau_{(a)}, \ \tilde{\tau}_{(a)}^{ab} = 0, \ \text{for } \{ab\} \neq 11 \quad \text{and} \quad \tilde{\mathbb{c}}_{(a)}^{1111} = \mathbb{c}_{(a)}, \ \tilde{\mathbb{c}}_{(a)}^{abcd} = 0, \ \text{for } \{abcd\} \neq 1111 \tag{45}$$

The global three-dimensional counterparts of the Kirchhoff stresses and associated moduli required at the macroscale are computed by

$$\tau_{(a)}^{ab} = Q_{(a)i}^{a}\, Q_{(a)j}^{b}\, \tilde{\tau}_{(a)}^{ij} \quad \text{and} \quad \mathbb{c}_{(a)}^{abcd} = Q_{(a)i}^{a}\, Q_{(a)j}^{b}\, Q_{(a)k}^{c}\, Q_{(a)l}^{d}\, \tilde{\mathbb{c}}_{(a)}^{ijkl} \tag{46}$$

Herein, the rotation matrix $\boldsymbol{Q}_{(a)}$ can be computed as a sequence of rotations first around the x_2-axis by $\vartheta_{(a)}$ and second around the x_3-axis by $\varphi_{(a)}$:

$$\boldsymbol{Q}_{(a)} = \boldsymbol{R}_{(a)}^{z}(\varphi_{(a)})\, \boldsymbol{R}_{(a)}^{y}(\vartheta_{(a)}) \tag{47}$$

DOI: 10.1002/nme

(cf. the definition of spherical coordinates given in Figure 1). The individual rotation matrices are given by

$$\boldsymbol{R}^{y}_{(a)} = \begin{bmatrix} \cos(\hat{\vartheta}_{(a)}) & 0 & \sin(\hat{\vartheta}_{(a)}) \\ 0 & 1 & 0 \\ -\sin(\hat{\vartheta}_{(a)}) & 0 & \cos(\hat{\vartheta}_{(a)}) \end{bmatrix}, \quad \boldsymbol{R}^{z}_{(a)} = \begin{bmatrix} \cos(\varphi_{(a)}) & -\sin(\varphi_{(a)}) & 0 \\ \sin(\varphi_{(a)}) & \cos(\varphi_{(a)}) & 0 \\ 0 & 0 & 1 \end{bmatrix}, \tag{48}$$

with $\hat{\vartheta}_{(a)} = \vartheta_{(a)} - \pi/2$. The two angles describing the actual orientation of the fibers can be identified by straightforward geometric calculations. Finally, after applying a pull-back operation ($\boldsymbol{\tau} \to \boldsymbol{S}$ and $\mathbb{c} \to \mathbb{C}$), the total second Piola–Kirchhoff stresses and moduli are obtained by

$$\boldsymbol{S} = \boldsymbol{S}^{\mathrm{iso}} + \sum_{a=1}^{n_f} \boldsymbol{S}_{(a)} \quad \text{and} \quad \mathbb{C} = \mathbb{C}^{\mathrm{iso}} + \sum_{a=1}^{n_f} \mathbb{C}_{(a)}, \tag{49}$$

wherein the stresses and moduli associated to the isotropic matrix are computed in a straightforward manner by $\boldsymbol{S}^{\mathrm{iso}} = 2\partial_{\boldsymbol{C}} \psi^{\mathrm{iso}}$ and $\mathbb{C}^{\mathrm{iso}} = 4\partial^2_{\boldsymbol{C}\boldsymbol{C}} \psi^{\mathrm{iso}}$.

4. APPLICATIONS AND NUMERICAL EXAMPLES

For the numerical examples provided in this section, we still have to define an explicit damage function and focus on the function given by

$$D(\alpha) = D_\infty \left[1 - \exp\left(-\frac{\alpha}{D_0} \right) \right] \tag{50}$$

(cf. Miehe [10]). Herein, $D_\infty \in \,]0, 1]$ denotes a maximal asymptotic limit value of the damage function and $D_0 > 0$ is a material parameter adjusting for the damage evolution velocity. Note that, although the damage function (50) fulfills $D < 0$ for physically relevant situations even for $D_\infty = 1$, we choose $D_\infty < 1$ for numerical reasons. Then, the explicit antiderivative reads

$$\bar{D}(\alpha) = D_\infty \left[\alpha + D_0 \exp\left(-\frac{\alpha}{D_0} \right) \right], \tag{51}$$

and the dissipation integral yields

$$\int_{t_k}^{t_{k+1}} \phi \, \mathrm{d}t = D(\alpha_{k+1})(\alpha_{k+1} + D_0) - D(\alpha_k)(\alpha_k + D_0) - D_\infty(\alpha_{k+1} - \alpha_k). \tag{52}$$

Finally, the incremental stress potential for damage evolution is obtained by

$$\begin{aligned} W(F) = {} & (1 - D)\psi^0(F) - (1 - D_k)\psi^0(F_k) \\ & + D(\alpha + D_0) - D_k(\alpha_k + D_0) - D_\infty(\alpha - \alpha_k). \end{aligned} \tag{53}$$

4.1. Mesh independence of the relaxed one-dimensional model

Here, two different effective hyperelastic strain energy functions are considered, and their response is compared with respect to the original incremental variational model and the relaxed representation. In detail, the St. Venant–Kirchhoff model, representing the special case of a linear stress–strain relation in a Lagrange formulation, and a compressible neo-Hooke model, showing a nonlinear response, are taken into account. The St. Venant–Kirchhoff model reads

$$\psi^0_{(\mathrm{SVK})} := \lambda/8(I_1 - 3)^2 + \mu/4\left(I_1^2 - 2I_1 - 2I_2 + 3\right), \tag{54}$$

with the Lamé constants λ and μ. The compressible neo-Hooke model is given by

$$\psi^0_{(\mathrm{NEO})} := \alpha_1 I_1 + \delta_1 I_3 - \delta_2 \ln\left(\sqrt{I_3}\right) \quad \text{with} \quad \delta_2 = 2\alpha_1 + 2\delta_1,\ \alpha_1 = \mu/2,\ \delta_1 = \lambda/4, \tag{55}$$

DOI: 10.1002/nme

wherein the Lamé-constants λ and μ are defined such that the model coincides with the linear theory for the linearized case at $F \approx 1$. Note that, for the one-dimensional representation, we set $\boldsymbol{F} = \mathrm{diag}\,[F, 1, 1]$, and then the invariants are obtained accordingly. In our analysis, we consider the parameters to have the values $\lambda = 0$, $\mu = 0.5$, $D_\infty = 0.99$, and $D_0 = 0.5$. As a first example, we analyze the response of the original incremental variational model and the relaxed formulation for both effective strain energy functions at the material point. The resulting stress–stretch response is shown in Figure 4. The main difference between the two models is the fact that the St. Venant–Kirchhoff model is not polyconvex, whereas the neo-Hooke model is polyconvex. The notion of polyconvexity in the sense of Ball [12, 13] plays a crucial role because this condition ensures the minimization of elastic variational functionals if coercive functions are considered.

However, as a result of the application of the damage model, both effective strain energy functions lead to a similar behavior, and even the model using the polyconvex effective energy lacks the loss of convexity at some point. A difference to the geometrically linear case is that the microbifurcation intensity d is not constant throughout the convexified region as it has been observed in Gürses [4] for small strains (see Figure 5(a.2,b.2)). This is a result of the differing interpolation ansatz (31), which has a multiplicative nature here. For the geometrically linear case, the bifurcation intensity is obviously constant for fixed bifurcation strains because of the additive structure of the interpolation ansatz. Because the volume fraction of the strongly damaged material ξ depends linearly on the deformation gradient, for fixed bifurcation deformation gradients, a linear increase is observed in Figure 5(a.1,b.1). Figure 6 shows the evolution of the damage variable D for the unrelaxed and the relaxed incremental variational model. Because, for the relaxed case, the main increase of damage is associated with a linear increase of volume fraction of strongly damaged parts in the material, the linear relationship is obtained after reaching the point of bifurcation initialization. Before that point, both models stay on the same path (cf. the magnified illustrations in Figure 6). As a second example, we consider a finite element calculation of a beam that is expanded in order to show the mesh

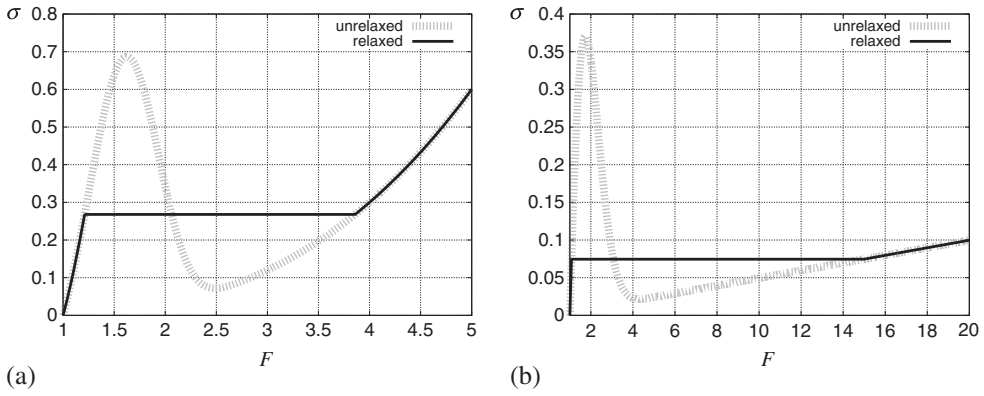

Figure 4. Stress–stretch diagram showing the response of the unrelaxed and the relaxed model for the (a) (non-polyconvex) St. Venant–Kirchhoff and (b) (polyconvex) neo-Hooke effective energy.

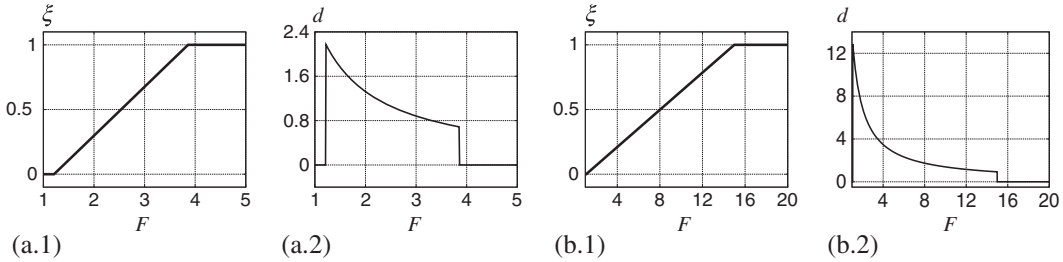

Figure 5. Evolution of bifurcation parameters ξ (1) and d (2) for the (a) (non-polyconvex) St. Venant–Kirchhoff and (b) (polyconvex) neo-Hooke effective energy.

DOI: 10.1002/nme

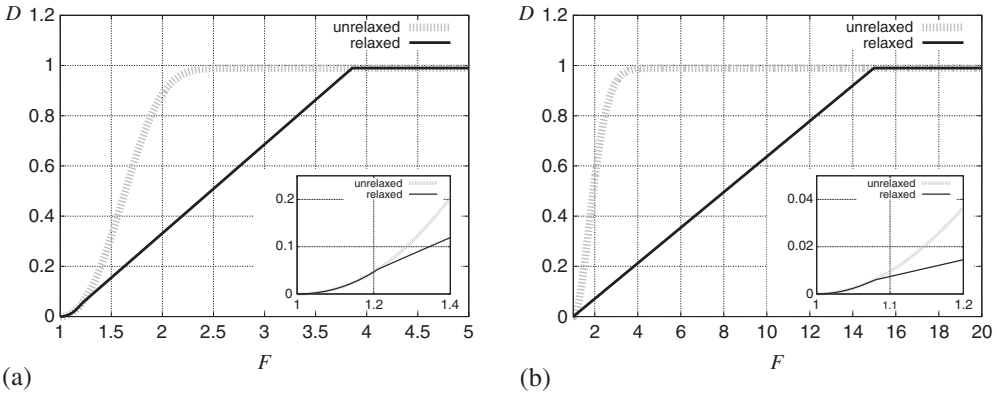

Figure 6. Damage–stretch diagram showing the response of the unrelaxed and the relaxed model for the (a) (non-polyconvex) St. Venant–Kirchhoff and (b) (polyconvex) neo-Hooke effective energy.

independency obtained when using the unrelaxed model. In order to introduce a distortion, the beam is composed of two serial truss elements $\mathcal{B}_1$ and $\mathcal{B}_2$ with linear ansatz functions where, in the second element, the first damage parameter is distorted and set to $D_\infty = 0.98999999$. The individual dimensions of the two elements are controlled by a domain parameter κ such that $l(\mathcal{B}_1) = (1-\kappa)\bar{l}$ and $l(\mathcal{B}_2) = \kappa\bar{l}$ with the total beam length $\bar{l}$. The truss cross section is set to 0.2 units of area, and the total length of the beam is 1.0 units of length. Then, tension is performed by fixing one side of the beam and applying a force p to the other such that the displacement u can be measured. The process is triggered numerically by controlling the arc length of the force–displacement curve. The resulting force–displacement curves are plotted in Figure 7. Although a relatively small distortion is applied, a strong distortion sensitivity is observed accompanied by an unphysical behavior in the postcritical domain of the tension test when using the original unrelaxed formulation. In contrast to this, a physically reasonable and mesh-independent response is obtained for the relaxed model.

4.2. Simulation of damage in microtruss materials

For achieving the goal of an ultralow density, improved impact absorption and high thermal conductivity materials with a significant porosity, often referred to as cellular solids, turn out to be quite efficient. As shown in Ashby [14], ordered open cellular structures are characterized by a higher stiffness compared with random open cellular structures because the mode of deformation

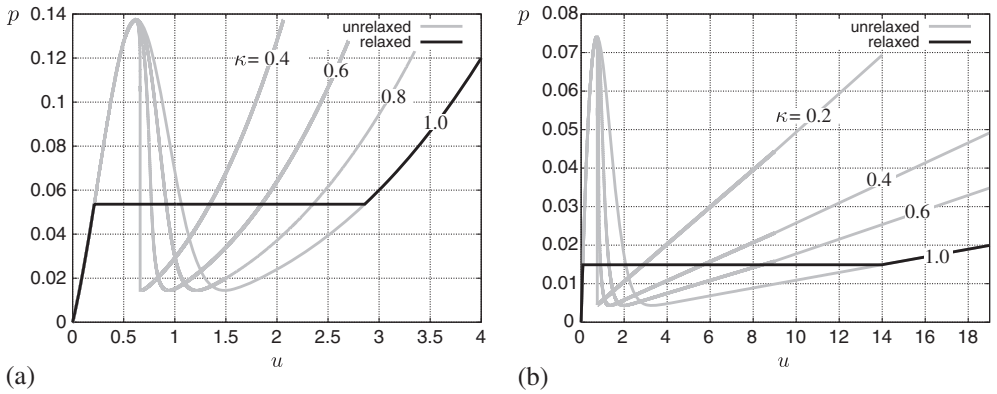

Figure 7. Force–displacement curves for distorted tension test. Variations of the domain parameter κ are depicted using the (a) St. Venant–Kirchhoff and (b) neo-Hooke effective energy. Note that the values of κ denote only the curves resulting from the original unrelaxed formulation; the relaxed model leads always to the same response no matter which distortion is applied.

DOI: 10.1002/nme

can be changed from bending dominated to stretch dominated; therefore, the power of the truss-like microstructure can be exploited. The resulting microtruss materials are basically composed of a periodic set of truss unit cells as exemplarily shown in Figure 8. In a variety of applications, microtruss materials made of polymers, which are commonly manufactured by lithographic techniques, are used. In this context, microstructures with unit cells even in the order of hundreds of nanometers and micrometers can be produced (see, e.g., Jacobsen *et al.* [15] and the references therein). Because of the nature of the polymer parent material, stress softening as a result of microscopic damage may occur in the individual microtrusses, leading to a macroscopically observable softening behavior. Therefore, in this section, we analyze the proposed relaxed variational damage formulation with respect to micro–macro calculations and investigate the impact on the homogenized macroscopic material response. For that purpose, the microtruss material from Figure 8 is considered and the unit cell shown in Figure 9(a) is identified (cf. Ashby [14]). The dimensions of the bordering box of the unit cell are $1 \times 1 \times 1$ length units and the cross section of the microtrusses is assumed to have circular shape with a radius of $r = 0.05$ length units. Then, two different virtual macroscopic tests, uniaxial tension in z-direction and simple shear in x-direction, are performed by prescribing linear displacement boundary conditions to the outer vertices of the unit cell in a displacement-driven process such that the associated macroscopic virtual test is obtained. The deformed unit cells are shown in Figure 9(b,c). Here, we consider deformable polymers where large deformations may be observed and restrict ourselves to the description of the softening behavior in the sense of the Mullins effect

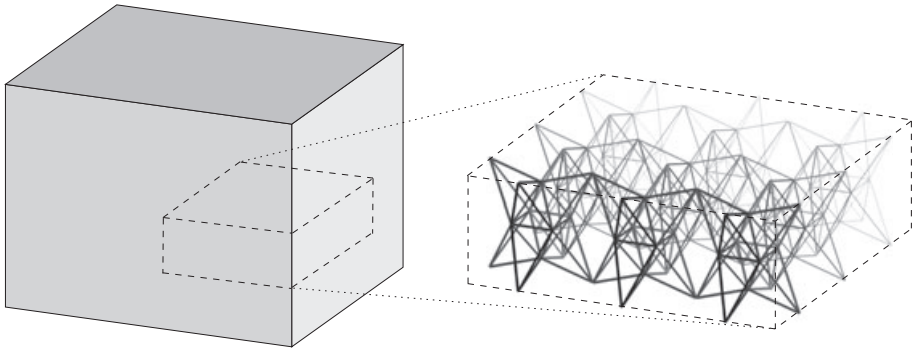

Figure 8. Example for a microtruss material with magnification of the microstructure. Note that this is a schematic illustration; typically, the truss elements are thicker compared with their length.

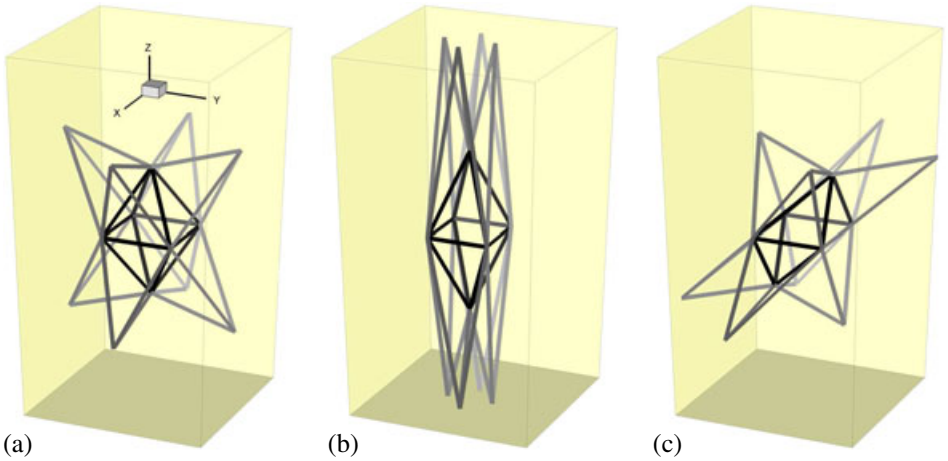

Figure 9. Microtruss unit cell in its (a) undeformed and deformed configuration due to the application of (b) uniaxial tension and (c) simple shear.

DOI: 10.1002/nme

(cf. Chagnon *et al.* [16]). Thus, we choose the Yeoh model for the description of the parent material leading to the effective strain energy function

$$\psi^0_{(\mathrm{YEO})} := c_1 \left(I_1 I_3^{-1/3} - 3 \right) + c_2 \left(I_1 I_3^{-1/3} - 3 \right)^2 + c_3 \left(I_1 I_3^{-1/3} - 3 \right)^3, \tag{56}$$

wherein the material parameters are set to $c_1 = 6.0$, $c_2 = 1.0$, and $c_3 = 900.0$ units of energy per volume. Note that, because all parameters are positive, the effective energy is polyconvex and therefore automatically rank-one convex. However, because of prepending, the damage term $(1-D)$ rank-one convexity is lost at a certain point. For the representation of the damage, the parameters $D_\infty = 0.99$ and $D_0 = 1.0$ are chosen. Then, the typical behavior showing the Mullins effect depicted in Figure 10(a) is obtained at moderate strains. First, a macroscopic uniaxial tension test is performed. The overall macroscopic stress–stretch response looks similar compared with the response obtained for the tensile tests of single truss elements. However, Figure 10(b) shows that a nonlinear macroscopic response occurs when the relaxed model is activated because of the interaction of the individual microtrusses. The influence of this interaction becomes clearer if a deeper analysis of the individual microtrusses is investigated. Therefore, now, the simple shear test is considered and the stress–stretch behavior in the truss elements where a loss of convexity occurs is analyzed (see Figure 11(b) for those elements). Note that the associated symmetric counterparts of these microtrusses are not depicted because no different stress–stretch behavior is observed there because symmetry. Figure 11(a) shows the microscopic stress in the individual truss elements σ versus the macroscopic stretch $\overline{F}_{zx}$. As can be seen, the individual microtrusses lose and recover convexity at different macroscopic strains. It is emphasized that, for the unrelaxed results, more than $8 \cdot 10^7$ incremental load steps are required in order to obtain more or less converging results, whereas the relaxed formulation needs only less than 1000. Even if such a high number of load steps is considered in the unrelaxed case, some of the truss elements suffer from convergence at some stretch states. As an example, this can be seen dramatically in element 2 at a macroscopic stretch of approximately $\overline{F}_{zx} \approx 1.7$, where the curve precipitates abruptly. Such convergence problems lead to distorted results even earlier than the loss of convexity is observed in the calculation where the relaxed model is considered. These individual points are marked as 'A' in Figure 11(a), whereas the loss of convexity is marked as 'B'; 'C' denotes the recovery of convexity. These numerical distortions are also observable in the macroscopic stresses, which are plotted versus the macroscopic stretches in Figure 11(c). A smooth macroscopic behavior is obtained due to the relaxed model again showing a nonlinear response whereas the unrelaxed model leads to a rather jagged response.

4.3. Simulation of damage in fiber-reinforced materials

Elastomeric materials reinforced by a single family of unidirectionally aligned fibers represent an important class of technological materials. One prominent example is that of tires, where usually

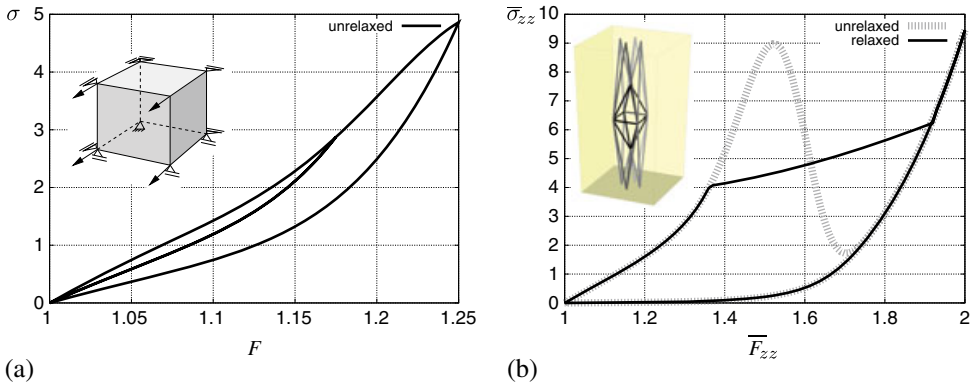

Figure 10. Uniaxial tension tests: (a) stress–stretch diagram of the parent polymer material and (b) homogenized macroscopic stress versus macroscopic stretch of the microtruss material.

DOI: 10.1002/nme

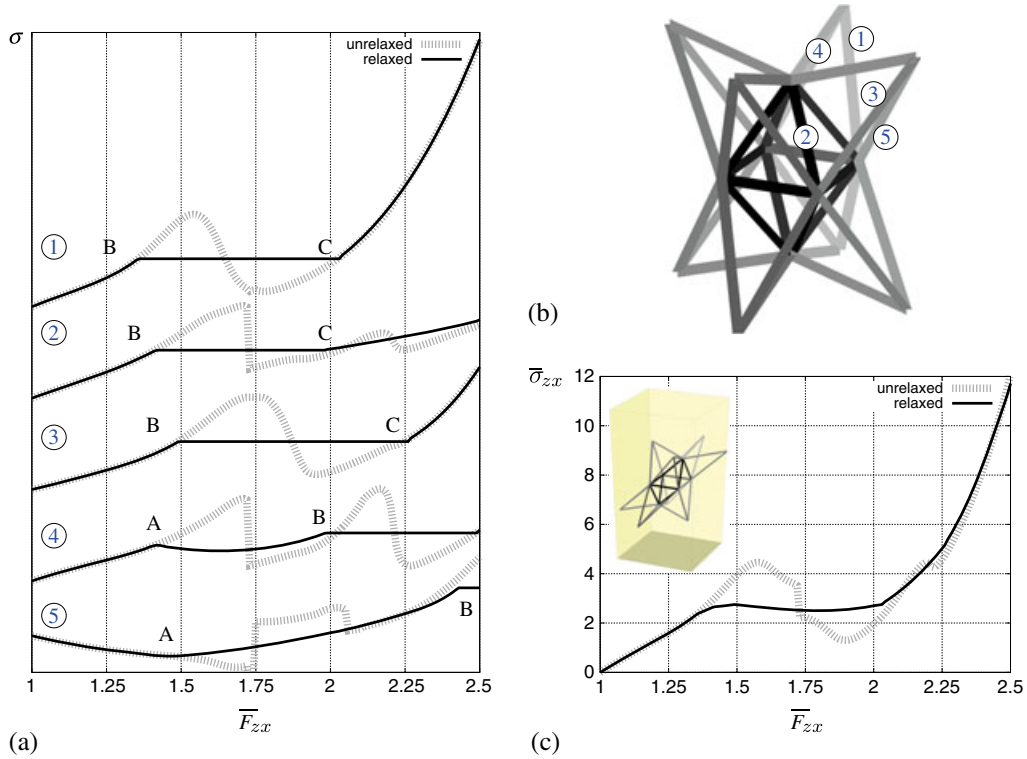

Figure 11. Simple shear test: (a) stress–stretch diagram of the individual truss elements where loss of convexity is observed, (b) declaration of those microtrusses, and (c) homogenized macroscopic stress versus macroscopic stretch of the microtruss material.

the radial plies are reinforced by polymer or steel cords in radial direction. In particular, the evolution of microstructure has started to gain scientific interest rather recently (see, e.g., Lopez-Pamies *et al.* [17]). Another important class of materials, where mainly two fiber families are incorporated in some matrix media, regards textile-reinforced membrane materials and soft biological tissues, for example, occurring in arterial walls. Here, two different numerical examples are considered, where we follow the approach for fiber-reinforced materials, which is described in Section 3.3.

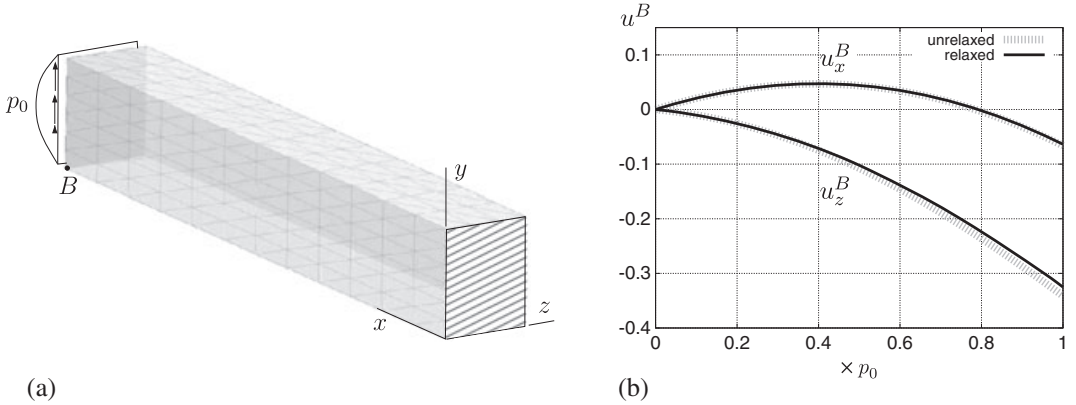

Figure 12. (a) Boundary value problem of a cantilever beam with fiber reinforcement in direction $\boldsymbol{A} = [0.707, 0.0, 0.707]^{\mathrm{T}}$ and (b) resulting displacement–load curves for point B and a maximal load of $p_0 = 5.5\mathrm{e}^{-4}$ force units; the beam has the dimensions $4 \times 1 \times 0.5$ units of length.

DOI: 10.1002/nme

4.3.1. Unidirectionally reinforced material. As a first example, we focus on a material that is reinforced by one fiber family, that is, $n_f = 1$. A cantilever beam with the dimensions $4 \times 1 \times 0.5$ units of length is subjected to a follower load, which is quadratically distributed over the height (cf. Figure 12(a)). The beam is discretized with 1332 tetrahedral elements by using the F-bar approach and quadratic ansatz functions for the displacements and a constant ansatz for the pressure. The external load given by $p_0 = 5.5d^{-4}$ is applied by incrementally increasing the load in 70 steps. Mesh and time convergence analysis showed that no significantly differing results are obtained when using more finite elements or finer time steps. In order to analyze the influence of the anisotropy governed by the presence of a unidirectional fiber reinforcement, the preferred direction in the reference configuration is prescribed as $\boldsymbol{A} = [\sin(\pi/4),\ 0,\ \cos(\pi/4)]^{\mathrm{T}}$. For the isotropic matrix material, the neo-Hooke model is considered using the parameters $\lambda = 0.3103$ and $\mu = 0.03448$ units of energy such that almost incompressibility is ensured. The unidirectional reinforcement is described by the Yeoh model with the parameters $c_1 = 6.0$, $c_2 = 1.0$, and $c_3 = 900.0$ units of energy, making use of the proposed variational formulation for damage with the parameters $D_\infty = 0.99$ and $D_0 = 0.001$. Two simulations, the one using the original damage model and the other using the relaxed formulation, are compared with each other. First, the displacement at point B is analyzed (see Figure 12(b)). As can be seen, the displacement in z-direction is tending strongly to the negative axis direction when increasing the load although axis-symmetric loads are applied. This is due to the fiber reinforcement leading also to a torsion of the beam around the x-direction and shows the strong anisotropy effect. This can be clearly observed in Figure 13, where the deformed configuration of the beam is shown at the maximal load level. There, the distribution of fiber damage is shown for the case where the original (unrelaxed) model is used (Figure 13(a)) and for the case where the relaxed formulation is applied (Figure 13(b)). The main observation is that the damage is mainly different at the fixed side of the beam because of a strongly localized character of the damage distribution there. This also leads to the loss of convexity of the original model in particular there, as illustrated in Figure 13(c). There, the elements where convexity is lost at least at one integration point are marked. A similar observation is made when comparing the von Mises–Cauchy stress distribution as depicted in Figure 14. There, the stresses are similar in the whole beam besides the locations where convexity is lost. In addition to that, Figure 12(b) shows that the displacement at point B is also quite similar

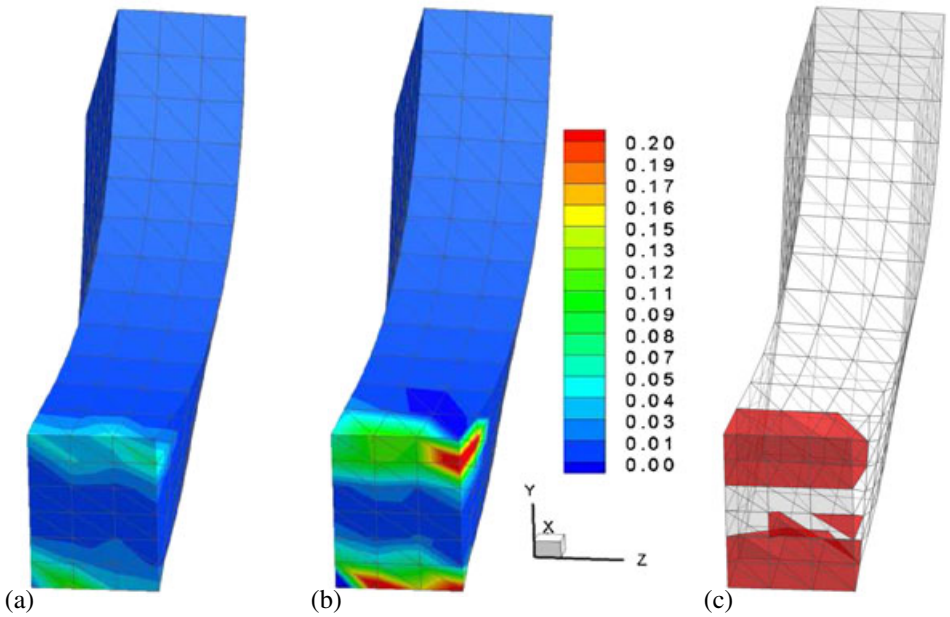

Figure 13. Deformed cantilever beam with distribution of fiber damage resulting from application of the (a) original (unrelaxed) and the (b) relaxed damage formulation and (c) illustration of elements where convexity of the original model is lost at least at one integration point.

DOI: 10.1002/nme

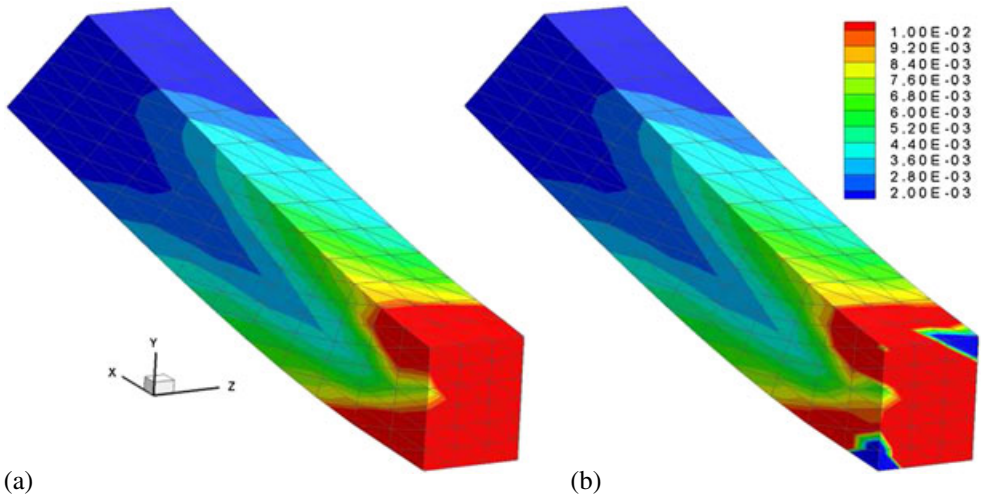

Figure 14. Deformed cantilever beam with distribution of von Mises–Cauchy stresses resulting from application of the (a) original (unrelaxed) and the (b) relaxed damage formulation.

for the unrelaxed and the relaxed formulation. This means that even if a different damage behavior resulting from the relaxed formulation may occur at some few locations where convexity is lost, the overall behavior is rather similar. However, because convexity is ensured at every point, existence of minimizers and material stability is guaranteed. Because significant compression and tension is obtained at the upper and lower parts of the clamp, respectively, this example shows that the proposed model can also be used in simulations where some areas where the reinforcement is under compression and some locations where the reinforcement is under tensile stresses occur.

4.3.2. Material with two fiber reinforcements. The second example takes into account the circumferential overstretch of an idealized healthy artery. Because, typically, arteries are modeled as thick-walled tubes with two superposed helically arranged fiber families, we consider again the structure of the strain energy function given in (43) and set $n_f = 2$. Healthy arteries consist of three layers, the intima, the media, and the adventitia. However, because of the relatively small thickness of the intima, this layer is not considered here. Because, typically, no damage is observed in the adventitia, damage evolution is only assumed in the media. In the media, the effective strain energy function for the fibers is chosen to be the well-known transversely isotropic function proposed in Holzapfel *et al.* [18]. The adaption to the one-dimensional formulation for the fiber reinforcement leads to the effective strain energy

$$\psi^0_{(\mathrm{HGO})} = \frac{k_1}{2k_2}\left[\exp\left(k_2\langle I_1 - 3\rangle^2\right) - 1\right], \tag{57}$$

wherein the Macauley bracket $\langle\cdot\rangle = (|\cdot| + (\cdot))/2$ filters out positive values. This ensures (i) that the effective strain energy is polyconvex and (ii) that the fibers carry only tensile stresses, which is commonly assumed in soft biological tissues. For the isotropic ground substance, the polyconvex neo-Hookean-type model

$$\psi^{\mathrm{iso}}_{(\mathrm{HGO})} = c_1\left(I_1\, I_3^{-1/3} - 3\right) + \epsilon_1\left(I_3^{\epsilon_2} + I_3^{-\epsilon_2} - 2\right) \tag{58}$$

(cf. Balzani *et al.* [19]) is considered. For the matrix the parameters $c_1 = 10.0$, $\epsilon_1 = 10.0$ units of energy per volume, and $\epsilon_2 = 5.0$ are used. The parameters for the fiber reinforcements are given by $k_1 = 80.0$, $k_2 = 100.0$, $D_\infty = 0.99$, and $D_0 = 10.0$; the fiber angle, that is, the angle between the fibers and the circumferential direction of the artery, is 43.39°. As shown in Figure 15(a), the typical behavior of arterial tissues (cf. Balzani *et al.* [19]) is obtained by these parameters. A stiffer behavior is observed in circumferential direction compared with that in the axial direction, which is due to the more circumferentially oriented fibers.

DOI: 10.1002/nme

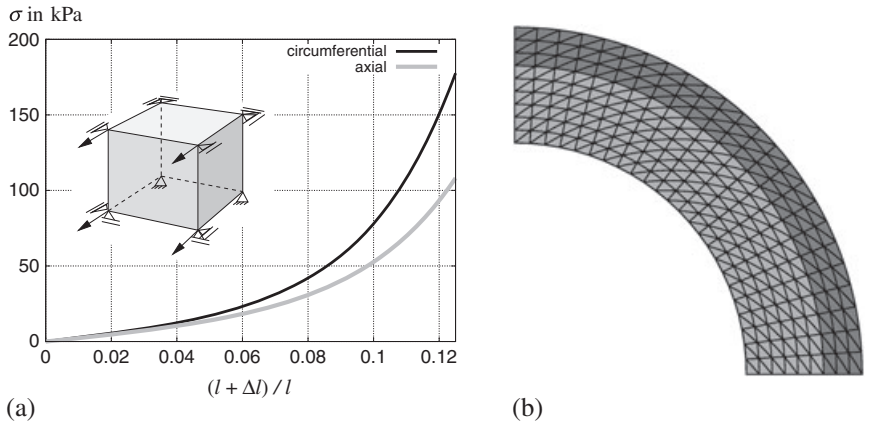

Figure 15. (a) Stress–strain diagram of a virtual constrained tension test performed in axial and circumferential directions by using the proposed model and (b) discretization of the considered quarter of a healthy artery. The length and the change of length of the test specimen in tension direction is denoted by l and Δl, respectively.

For the modeling of the adventitia where no damage is assumed, the model and the parameters used in Schröder *et al.* [20, Section 5.2.2] are applied. Because of the rotation symmetry, only one quarter of the cross section is considered. The geometric model of the considered arterial cross section is shown in Figure 15(b). The inner radius is chosen as 3 mm, and the thickness of the media and adventitia are given as 1 and 0.5 mm, respectively. For the discretization, a total number of 456 six-noded triangular elements are taken into account. In order to account for the symmetry conditions, the displacements at the lower nodes are fixed in vertical direction and at the left nodes in horizontal direction. Then, an internal pressure p is applied by attaching quadratic surface load elements to the inner side of the artery. A blood pressure of 120 mmHg is assumed to be physiological, and higher pressures are considered to represent circumferentially overstretched situations, where a significant damage should be expected in the media. Figure 16(a) shows the distribution of the damage variable $D_{(1)}$ for three different loading situations where $p = 200$ mmHg, $p = 300$ mmHg, and $p = 375$ mmHg. It can be observed how the damage evolves because of an increasing internal pressure. In Figure 16(b), the area where the original model loses convexity; thus, the relaxed formulation is activated. Because of the increasing damage values with increasing internal pressure also, the area spreads where the relaxed model is active.

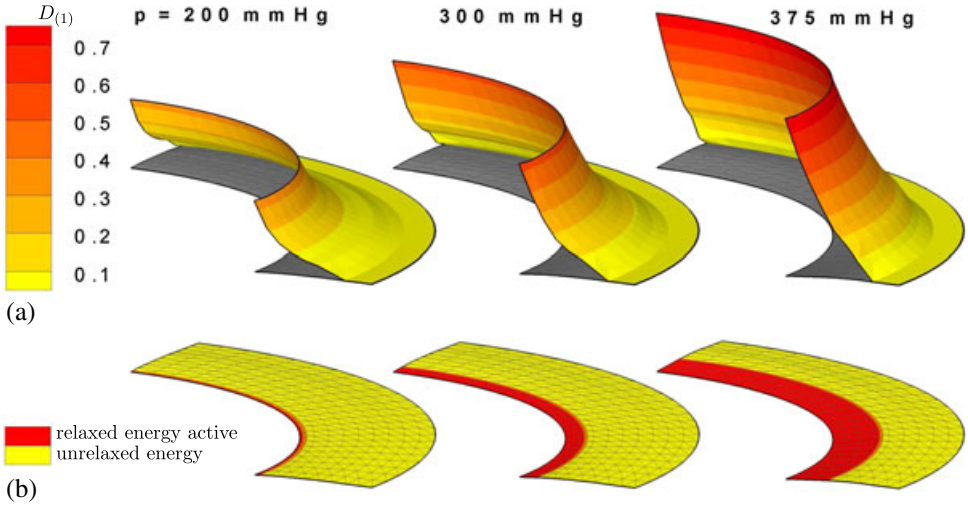

Figure 16. (a) Distribution of the damage variable $D_{(1)}$ and (b) illustration of the regime where the relaxed formulation is activated.

DOI: 10.1002/nme

It should be remarked that this simulation is only a qualitative example showing that the proposed model is also applicable to the problem of arterial overstretching. The results do not, of course, claim to be realistic because, for example, eigenstresses are not taken into account, and in addition to that, the material parameters were not adjusted to experiments but rather chosen such that a qualitatively reasonable response is obtained.

5. CONCLUSION

A relaxed incremental variational formulation for damage at large strains has been presented. The model founds on the continuum damage mechanics and takes into account a standard formulation as long as the incremental stress potential is convex. As soon as convexity is lost, the initially homogeneous material is assumed to bifurcate into a weakly and strongly damaged phase. Then, a relaxed stress potential, which is mainly obtained by a geometric construction of an interpolation between the two bifurcated states, is considered. Thereby, the resulting model can be interpreted as the homogenization of the microheterogeneous distribution of weakly and strongly damaged phases. The main advantage of this method is that existence of minimizers of the variational problem is ensured, which might also play an important role with respect to numerical calculations. Because, in various materials, fiber-like or truss-like elements that undergo damage during deformation occur at the microscale, the consideration of a one-dimensional relaxed damage formulation for the directional elements turned out to be efficient. Therefore, the special one-dimensional case has been derived and an algorithmic framework has been presented. Furthermore, a model for fiber-reinforced materials was proposed on the basis of a local transformation of the deformations into the fiber directions, evaluation of the relaxed damage model, and then transforming the stresses and moduli back to the three-dimensional space. Several numerical examples showed the performance of the model. First, mesh independency of the one-dimensional model was shown. Then, the numerical homogenization of a microtruss material was investigated, where it was shown that the unrelaxed formulation suffers from convergency problems in individual microtrusses even for a high number of time steps, whereas the relaxed formulation leads to converging results at a reasonable number of time steps. Next, a fiber-reinforced cantilever beam was simulated, where the impact of the anisotropy due to the fiber reinforcement lead to an unsymmetric deformation. Furthermore, it was shown that the relaxed formulation leads to similar results as the unrelaxed one when only some few material points lose convexity. However, convexity and therefore existence of minimizers is ensured by the proposed formulation. As a last example, the circumferential overstretch of an idealized artery was simulated, and the evolution of the relaxed damage formulation was illustrated. Although the results cannot be interpreted as quantitatively realistic, they show the applicability to arterial wall simulations. If more reliable numerical analysis are to be performed, the model has be adapted to the special class of soft biological tissues and adjusted to cyclic tests of layer-specific experiments. This remains to be done in future publications.

APPENDIX A

For the calculation of the local nonconvex minimization problem, that is, the solution of the necessary condition given in (37) in terms of the Newton method, the derivatives in (38) have to be computed by

$$\begin{aligned}
\partial_d \bar{W} &= \xi(1-\xi)(P^+ - P^-)\, F, \\
\partial_\xi \bar{W} &= W^+ - W^- - d\,[\xi P^+ + (1-\xi) P^-]\, F, \\
\partial^2_{dd} \bar{W} &= \xi(1-\xi)[(1-\xi)\mathbb{A}^+ + \xi \mathbb{A}^-]\, F^2, \\
\partial^2_{\xi\xi} \bar{W} &= 2d(P^- - P^+)\, F + d^2[\xi \mathbb{A}^+ + (1-\xi)\mathbb{A}^-]\, F^2, \\
\partial^2_{d\xi} \bar{W} &= (1-2\xi)(P^+ - P^-)\, F - d\,\xi(1-\xi)(\mathbb{A}^+ - \mathbb{A}^-)\, F^2 = \partial^2_{\xi d} \bar{W},
\end{aligned} \tag{A.1}$$

wherein the abbreviations $W^+ := W(F^+)$, $W^- := W(F^-)$, $P^+ := P(F^+)$, $P^- := P(F^-)$, $\mathbb{A}^+ := \mathbb{A}(F^+)$, and $\mathbb{A}^- := \mathbb{A}(F^-)$ are used. Herein, the stress and tangent terms are

DOI: 10.1002/nme

calculated by evaluating the relations (33) and (34) at the individual bifurcated deformation gradients F^+ and F^-. For the calculation of the tangent moduli associated with the convexified energy, the derivatives given in (A.1) and further second derivatives, which are given in the following equation, are required:

$$\begin{aligned}
\partial^2_{Fd}\bar{W} &= \xi(1-\xi)\,F\,(\mathbb{A}^+ - \mathbb{A}^-) + \xi(1-\xi)(P^+ - P^-) \\
&\quad + \xi(1-\xi)\,F\,d\,[(1-\xi)\mathbb{A}^+ + \xi\mathbb{A}^-], \\
\partial^2_{F\xi}\bar{W} &= P^+ - P^- - Fd[\xi\mathbb{A}^+ + (1-\xi)\mathbb{A}^-] + (1-2\xi)\,d\,(P^+ - P^-) \\
&\quad - \xi(1-\xi)\,Fd^2\,(\mathbb{A}^+ - \mathbb{A}^-), \\
\partial^2_{FF}\bar{W} &= \xi\mathbb{A}^+ + (1-\xi)\mathbb{A}^- + 2\xi(1-\xi)\,d\,(\mathbb{A}^+ - \mathbb{A}^-) \\
&\quad + \xi(1-\xi)\,d^2[(1-\xi)\mathbb{A}^+ + \xi\mathbb{A}^-].
\end{aligned} \tag{A.2}$$

ACKNOWLEDGEMENTS

The financial support of the 'Deutsche Forschungsgemeinschaft' (DFG), project no. BA 2823/6-1, is gratefully acknowledged.

REFERENCES

1. Francfort GA, Marigo JJ. Stable damage evolution in a brittle continuous medium. *European Journal of Mechanics, A/Solids* 1993; **12**:149–189.
2. Francfort GA, Garroni A. A variational view of partial brittle damage evolution. *Archive of Rational Mechanics and Analysis* 2006; **182**:125–152.
3. Francfort GA, Marigo JJ. Revisiting brittle fracture as an energy minimization problem. *Journal of the Mechanics and Physics of Solids* 1998; **46**:1319–1342.
4. Gürses E. Aspects of energy minimization in solid mechanics: evolution of inelastic microstructures and crack propagation. *Ph.D. Thesis*, Bericht Nr.: I-19, Institut für Mechanik (Bauwesen), Lehrstuhl I, Professor Dr.-Ing. C. Miehe, 2007.
5. Miehe C. Strain-driven homogenization of inelastic microstructures and composites based on an incremental variational formulation. *International Journal for Numerical Methods in Engineering* 2002; **55**:1285–1322.
6. Dmitrievic BJ, Hackl K. A method for gradient enhancement of continuum damage models. *Technische Mechanik* 2008; **28**:43–52.
7. Ortiz M, Repetto EA. Nonconvex energy minimization and dislocation structures in ductile single crystals. *Journal of the Mechanics and Physics of Solids* 1999; **47**:397–462.
8. Ortiz M, Stainier L. The variational formulation of viscoplastic constitutive updates. *Computer Methods in Applied Mechanics and Engineering* 1999; **171**:419–444.
9. Silhavý M. *The Mechanics and Thermodynamics of Continuous Media*. Springer-Verlag: Berlin Heidelberg, 1997.
10. Miehe C. Discontinuous and continuous damage evolution in Ogden-type large-strain elastic materials. *European Journal of Mechanics, A/Solids* 1995; **14**:697–720.
11. Balzani D, Schröder J, Gross D. Simulation of discontinuous damage incorporating residual stresses in circumferentially overstretched atherosclerotic arteries. *Acta Biomaterialia* 2006b; **2**(6):609–618.
12. Ball JM. Constitutive inequalities and existence theorems in nonlinear elastostatics. In *Heriot-Watt Symposium*, Vol. 1, Knops RJ (ed.). Pitman: London, 1977a.
13. Ball JM. Convexity conditions and existence theorems in non-linear elasticity. *Archive for Rational Mechanics and Analysis* 1977b; **63**:337–403.
14. Ashby MF. The properties of foams and lattices. *Philosophical Transactions of the Royal Society A* 2006; **364**:15–30.
15. Jacobsen AJ, Barvosa-Carter W, Nutt S. Micro-scale truss structures formed from self-propagating photopolymer waveguides. *Acta Mechanica* 2007; **19**:3892–3896.
16. Chagnon G, Verron E, Gornet L, Marckmann G, Charrier P. On the relevance of continuum damage mechanics as applied to the Mullins effect in elastomers. *Journal of the Mechanics and Physics of Solids* 2004; **52**:1627–1650.
17. Lopez-Pamies O, Idiart MI, Li Z. On mirostructure evolution in fiber-reinforced elastomers and implications for their mechanical response and stability. *Journal of Engineering Materials and Technology* 2011; **133**:011007–1 –011007–10.
18. Holzapfel GA, Gasser ThC, Ogden RW. A new constitutive framework for arterial wall mechanics and a comparative study of material models. *Journal of Elasticity* 2000; **61**:1–48.
19. Balzani D, Neff P, Schröder J, Holzapfel GA. A polyconvex framework for soft biological tissues. Adjustment to experimental data. *International Journal of Solids and Structures* 2006a; **43**(20):6052–6070.
20. Schröder J, Wriggers P, Balzani D. A new mixed finite element based on different approximations of the minors of deformation tensors. *Computer Methods in Applied Mechanics and Engineering* 2011; **200**:3583–3600.

DOI: 10.1002/nme